Slipping-Free Halide Perovskite Supercrystals from Supramolecularly-Assembled Nanocrystals

Takuya Okamoto,[a,b] Vasudevanpillai Biju*[a,b]

[a]Research Institute for Electronic Science, Hokkaido University, Sapporo, Hokkaido 001-0020, Japan; [b]Graduate School of Environmental Science, Hokkaido University, Sapporo, Hokkaido 001-0020, Japan

*Corresponding Authors: biju@es.hokudai.ac.jp

Abstract: Supramolecularly assembled high order supercrystals (SCs) help control the dielectric, electronic, and excitonic properties of semiconductor nanocrystals (NCs) and quantum dots (QDs). Ligand-engineered perovskite NCs (PNCs) assemble into SCs showing shorter excitonic lifetimes than strongly dielectric PNC films showing long photoluminescence (PL) lifetimes and long-range carrier diffusion. Monodentate to bidentate ligand exchange on ca. 8 nm halide perovskite ($APbX_3$; A:Cs/MA, X:Br/I) PNCs generates mechanically stable SCs with close-packed lattices, overlapping electronic wave functions, and higher dielectric constant, providing distinct excitonic properties from single PNCs or PNC films. From fast Fourier transform (FFT) images, time-resolved PL, and small-angle X-ray scattering (SAXS), we identify structurally and excitonically ordered large SCs. An Sc shows a smaller spectral shift (<35 meV) than a PNC film (>100 meV), a microcrystal (>100 meV), or a bulk crystal (>100 meV). Also, the exciton lifetime (<<10 ns) of an SC is excitation power-independent in the single exciton regime $\langle N \rangle < 1$, comparable to an isolated PNC. Therefore, bidentate-ligand-assisted SCs help overcome delayed exciton or carrier recombination in halide perovskite nanocrystal assemblies or films.

1. Introduction

Lead halide perovskites (LHPs) show excellent optical and electronic properties.[1] Controlling the excitonic carrier lifetimes of LHPs is important for tuning their applications. Isolated PNCs show short Auger lifetimes due to strongly confined excitons.[1,2] PNCs are in the film or assembled state in various optical and photovoltaic devices. However, PNC assemblies show unusually long-range carrier diffusion due to dielectric screening,[1d,3] exciton-dressing,[4] excited state electron wavefunction overlapping, and the photon propagation effect (reabsorption).[1e,5] Furthermore, exciton splitting, hole trapping, and delayed non-geminate recombination affect the electronic properties of these assemblies.[6] The long carrier lifetime of PNC self-assemblies becomes short at high excitation intensities due to an exponential increase in the non-geminate recombination rate.[7] Such uncontrolled carrier diffusion and recombination are undesired for optoelectronic applications.

Recently, perovskite SCs have become attractive for superfluorescence (SF), low-threshold light amplification, and aggregation-induced PL intensity enhancement (AIE).[8] SF by cooperative emission with red-shifted PL and short PL time was detected at the liquid helium temperature.[9] Zhou et al. demonstrated cavity-enhanced SF with picosecond pulse duration in a perovskite QD (PQD) superlattice (SL) microcavity.[9b] Lasing and amplified spontaneous emission (ASE) from perovskite SCs have also been studied due to their significance to photonic crystals.[10] A templated $CsPbBr_3$ assembly showed ASE under lower optical excitation fluences than a PNC film.[10b] Also, AIE was reported for self-assembled low-dimensional perovskite SCs.[11] Bi et al. reported the self-assembly of $CsPbBr_3$ nanoplatelets into cuboid crystals[11b] with the PL quantum yield increase from 50 to 91% and a PL redshift. PL redshifts and PL lifetime changes of SCs compared to isolated PNCs are caused by the combined dielectric environment, electronic coupling, and

photon propagation effects.[12] The optical and electronic properties of PNCs depend on the strength of exciton confinement and the degree of dielectric screening tuned by the size and shape of the assembly.[13] The optical properties of PNC films and SCs depend on the electronic structures of excitons.[1d,1g,3,7] Unlike a PNC film, showing largely red-shifted PL and a long PL lifetime, electronic coupling among assembled PNCs introduces minibands in an SC.[12b,14] The degree of the electronic coupling strongly depends on the interparticle distance[15] and alignment in an SC.[16] Nevertheless, PNC dislocation and structural stability of SCs formed by the self-assembly of simple ligands remain unresolved.

Due to the large surface energy, quantum-sized perovskite materials spontaneously self-assemble into ordered structures and SCs.[11a-c,17] Monodentate hydrophobic ligand-capped PNCs assemble by the van der Waals interactions, which is also accelerated by solvent evaporation,[8,12a,14c] antisolvent addition,[11c,18] or surface modification.[9c,10a,19] Also, templates such as oil-in-oil droplets,[9d,20] boron silicate glass networks,[21] and polymer molds help form SCs.[10b] For example, Tang et al. demonstrated isotropic SCs using oil-in-oil templates.[20] Cherniukh et al. prepared spherical SCs from $CsPbBr_3$ nanocubes using a microdroplet template.[9d] Wang et al. prepared self-assembled cubic SCs using L-cysteine.[22] Li et al. synthesized cuboid and spindle-shaped perovskite SCs by photoinduced alkynyl homocoupling.[23] Nevertheless, a correlation among the structures, stability, optical properties, and exciton and carrier recombination processes of isolated, close-packed, and SC perovskites is missing. We found PNCs self-assembled by monodentate ligands deform under mechanical stress, dislocating PNCs, decreasing the local dielectric constant, and changing the PL color and lifetime. Although the mechanical stability of SCs formed by weak interactions among monodentate ligands is yet to be rationalized, we hypothesize and demonstrate mechanically stable, slipping-free halide

perovskite ($APbX_3$; A:Cs/MA, X:Br/I) SCs with long-range ordering by interlocking PNCs using the bidentate ligand eicosanedioic acid (EA, Figure 1). The structures and excitonic properties of the SCs are compared with monodispersed PNCs and self-assembled PNC films. STEM images and SAXS clarify long-range 2D and 3D SCs. The bidentate ligand-assisted SCs are free from mechanical slipping, exciton splitting, spectral shifts, and prolonged PL lifetimes typical to PNC films. The close-packed PNC structure with overlapping electronic wave functions and a higher dielectric constant brings unique excitonic properties to an SC. Time-resolved PL measurements help correlate the PL wavelengths, miniband formation, and excitonic and non-geminate carrier recombination rates of the SC.

2. Results and Discussion

We synthesized the PNCs ($APbX_3$; A:Cs/MA/FA, X:Br/I) with oleic acid (OA) and hexadecyl amine ligands. Synthesis and characterization of the PNCs are in the supporting information. Figure 1a shows the absorption and PL spectra of monodispersed $CsPbBr_3$ and $CsPbI_3$ PNCs. For the as-synthesized cubic PNCs (8.4±0.9 nm, Figures 1b, S1, and S2), the excitonic and PL peaks are at 496 and 509 nm for the bromide and 670 and 675 nm for the iodide samples, respectively. PNC films were prepared by drop-casting PNC colloidal solutions (1 mg mL^{-1}) on a glass slide. Figure S3 shows the top-view and cross-section SEM images of a $CsPbBr_3$ PNC film. The average thickness of the film is 1.2 μm. We prepared $APbX_3$ SCs by a ligand-exchange-assisted sedimentation technique [Figure 1c(i)]. EA [Figure 1c(ii)] with the -COOH groups at both ends coordinates to the PNCs in an SC, which is more advantageous for inter-PNC linking than monodentate ligands. After adding an EA solution in toluene (0.5 mM, 2 mL) to a PNC solution, the OA ligands were exchanged with EA spontaneously until the ligand concentration attained equilibrium between the absorbing and desorbing ligands in about 48h [Figure 1c(iii)]. Figure 1d

shows PNC colloids (i) without and (ii) with adding the EA solution under room light and UV light. The PNCs without EA continued as a stable dispersion for more than 48 h [Figure 1d(i)], whereas most of the PNCs were settled as SCs after adding the EA solution [Figure 1d(ii)]. After discarding the supernatant and washing the SCs using an EA solution, $CsPbBr_3$ SCs were collected and deposited on TEM grids and glass coverslips for STEM, SEM, XRD, and PL measurements. Common SCs are rectangle-shaped (Figure 2a,b). The assembled $CsPbBr_3$ PNCs in an SC are well-aligned. The sizes of PNCs in the SCs are estimated at 8.1±1.0 nm (Figure S1b), showing the ligand exchange does not affect the PNC size. The FFT images of an SC (Figure 2c,e) and a self-assembled monolayer (Figure 2d) indicate a homogenous four-fold symmetry due to close-packed cubic PNCs. STEM (Figure 2c) and SEM images (Figure 2e) confirm well-ordered PNCs in SCs. While $CsPbBr_3$ and $CSPbI_3$ (Figures 2 and S4) form short-range assemblies, $MAPbX_3$ PNCs form irregular assemblies. In contrast, a PNC film shows a homogenous circular FFT pattern, indicating a random arrangement of PNCs (Figure 2f). Also, partially assembled and fused PNCs were observed in films (SEM image, Figure 2f). Interestingly, the constituent PNCs in an SC are periodically arranged by EA. Also, unlike short-range ordered PNC arrangements in a film, long-range arrangements were evident from SEM and STEM images (Figure 2c,e). Nevertheless, MA and FA-based PNCs formed irregular assemblies, which need further attention.

We measured XRD and SAXS data to evaluate the structures, alignment, and interparticle distances in PNC films and SCs. Figure 3a,b shows the XRD patterns of a PNC film and SCs, which help assign cubic unit cells with $Pm\bar{3}m$ space group to the PNCs.[1f,7] After the SC formation, the XRD patterns remained unchanged, indicating that the PNC crystal structure did not change in the SC. Figure 3a (inset) shows the SAXS patterns of PNCs and an SC. The SAXS peak at $q = 0.5$ nm^{-1} indicates 3.5 nm inter-PNC spacing in a film, consistent with the STEM data (Figure 2d).

The SAXS pattern of the SC sample matches the peak at q = 0.5 nm^{-1} for a film, confirming the close-packed PNC structure.

Time-resolved PL (TRPL) measurements help us to correlate the structure-property relations of isolated PNCs, PNC films, and SCs. Figure 3c,d shows PL spectra and decay curves of an isolated $CsPbBr_3$ PNC, a PNC film, and an SC, with the PLwavelengths centered at 511, 518, and 534 nm, respectively. The PL spectra and decays of $CsPbBr_3$ and $CsPbI_3$ SCs are compared in Figure S5. The PL decay curves were fitted using the triexponential kinetics (Table S1). Isolated PNCs show shorter average PL lifetimes (<5 ns) due to strongly confined excitons; the effective Bohr diameter for a $CsPbBr_3$ NC is 7 nm.[24] Conversely, PNC films show much longer PL lifetimes (>175 ns) with largely red-shifted (>100 meV) PL spectra relative to a PNC. The long PL lifetime and red-shifted emission of a PNC film (Figure 3c) are due to weak dielectric screening and photon reabsorption-emission, like in bulk films or crystals.[1e,25] Exciton splitting into free charge carriers under strong dielectric screening in self-assembled films and fused lattices with stripped ligands leads to delayed radiative non-geminate recombination.[3,7,11c] Furthermore, the excited state lifetime and optical bandgap of a PNC sample are determined by the band-edge electronic structure, defects, and trapping-detrapping processes.[25]

Compared to a PNC film, the small surface-to-volume ratios of SCs suppress surface-related nonradiative recombination and delayed recombination.[11c] The PL redshift is much smaller (<35 meV, Figures 3c and S5a) for an SC than a PNC film or fused PNCs (>100 meV). Also, the PL lifetime of an SC (<10 ns, Figure 3d) is comparable to isolated PNCs, but much shorter than a PNC film (>100 ns), suggesting the dielectric exciton screening by the surrounding bidentate ligands in an SC is greater than a PNC film but weaker a bulk crystal. Although defect-assisted nonradiative recombination and inter-PNC charge transfer accelerate the relaxation,[16] narrowly

distributed PL lifetimes (7 to 8.1 ns or 8.8 to 9.7 ns, Figure S6) indicate a uniform low defect density in an SC. The optical bandgap (ca. 2.393 eV) and PL lifetimes (<10 ns) of SCs suggest minimal reabsorption emission in the PL spectra or decay profiles due to a small number of PNCs in an SC.[12] Therefore, we assume interparticle electronic coupling as the main ruler for the PL spectral maximum and lifetime of SCs.

Figure 4 shows excitonic/carrier recombination processes in photoexcited PNC samples. Inter-PNC electronic coupling generates minibands with a lower conduction band minimum than isolated PNCs [Figure 4b(iii)],[12b,14a] like strong electronic coupling reported for ordered semiconductor SCs.[15,16] We call the Kroning-Penney model[26] to validate the band-edge modification manifested by the spectral shift of SCs. Accordingly, the bandgap of the SC is given by eq. 1, which is provided by eq. 2 for a PNC.

$$E_g^{SC}(n) = E_g^{3D} + E_e(n, q = 0) + E_h(n, q = 0) \quad (1)$$

$$E_g^{NC}(n) = E_g^{3D} + E_e(n \to \infty, q = 0) + E_h(n \to \infty, q = 0) \quad (2)$$

where, E_g^{3D} is the bulk bandgap, E_e and E_h are electron and hole energies, n is the carbon number of a ligand (spacing), and q is the wave number ($2\pi n/L$). For a bulk crystal ($n \to 0$), electrons or holes do not contribute to bandgap changes. The bandgap change (ΔE = 32 meV) detected for the SCs is comparable to the simulated value (ΔE = 2 to 28 meV)[26] for SCs using this model.

When fused PNC lattices are prepared by ligand stripping, a high-quality PNC film that avoids ligand stripping and lattice fusion carries excess ligands.[11c] Such noncoordinating ligands hamper long-range PNC ordering and engage PNCs to slip under a mechanical force ($\geq$ 5 N, Figure S7), causing a PL spectral blueshift (526 to 518 nm, Figure 4c) and a PL lifetime decrease (106 to 84 ns). In contrast, an SC with PNCs interlocked by the bidentate ligand is free from slipping, PL spectral blueshift, and PL lifetime decrease under mechanical stress (ca. 5 N, Figures 4d and S8).

Conversely, the mechanically stressed SC shows a red-shifted PL spectrum and a longer PL lifetime (Figure S5). These changes are attributed to the disordering of surface PNCs, providing partial film-like characteristics only to the SC surface.

Excitation-power-dependent photocounts, correlated with PL lifetimes, help clarify the short PL lifetime or the delayed emission suppression in an SC, unlike a PNC film. The laser fluence is converted into an excitonic occupation $\langle N \rangle$[27] obtained from eq. 3.

$$\langle N \rangle = (\text{Laser fluence} \times \text{Absorption cross-section})/h\nu \qquad (3)$$

The absorption cross-section value for a $CsPbBr_3$ PNC (d = 8 nm) is estimated at 4.5×10^{-14} cm^2.[10a,28] The exciton recombination rates for an SC and a PNC film were measured in the single-exciton regime $\langle N \rangle << 1$. The PL intensity (photocounts, I_{PL}) shows the following relationship (eq. 4) with the excitation power (I_{ex}),[29]

$$I_{PL} = A\, I_{ex}^{k} = B\, \langle N \rangle^{k} \qquad (4)$$

where A and B are constants. The exponent k is related to the radiative recombination mechanism. For a PNC film, the I_{PL} increases linearly (k = 0.92) with increasing $\langle N \rangle$ (Figure 4e). In contrast, the I_{PL} increases linearly (k = 1.03) and saturates ($\langle N \rangle > 0.03$) for an SC. The k values ca. 1 indicate single exciton radiative recombination. For the excitation power dependency ofthe PL lifetime, the τ value continuously decreases from 186 to 36 ns for a PNC film (Figure 4f). The long PL lifetime of a PNC film at low I_{ex} values suggests strong dielectric screening of excitons, followed by free carrier generation.[7,11c] As the I_{ex} is increased, inter-carrier interaction is increased. In contrast, an SC shows the constant τ for $\langle N \rangle < 0.03$ (Figure 4f). The excitation power independent short PL lifetime of an SC in the single-exciton regime ($\langle N \rangle < 1$) suggests its single PNC-like behavior, with strong exciton confinement rather than exciton splitting and free carrier generation. Therefore,

bidentate ligands interlock PNCs in an SC and prevent PNC fusion or slipping, unlike ligand-stripped perovskite lattices or PNC films.

Previous reports show large PL redshifts (>150 meV) for perovskite SCs formed by self-assembly without ligand exchange.[12a,14a-c,20,23] The PL lifetime also varies with spectral shifts. Li et al. reported large PL redshift ($\Delta\lambda$ = 28 nm) and a longer PL lifetime (from 7.1 for a PNC to 37.9 ns for the SC) for $CsPbBr_3$ SCs formed by a photoinduced alkyl homocoupling among PNCs[23]. Kanemitsu et al. recently reported excitonic lifetime change in perovskites by exciton coupling with phonons and polarons.[30] Not all perovskite SCs show red-shifted PL or longer PL lifetimes. Lapkin et al. reported a PL blueshift and a PL lifetime decrease for SCs compared to isolated PNCs,[31] where the PL properties of SCs are affected by the PNC alignment, the SC preparation temperature, local environments, and aging. The excitonic properties of SCs are correlated with the compressive strain of PNCs in soft ligand shells.[9c,14b,d,18,31] The SCs prepared in this work show stability against mechanical stress, unlike a PNC film, which is attributed to PNC interlocking and ordering in an SC by the bidentate EA, which also protects PNCs from fusion. Also, the SCs are free from exciton splitting and uncontrolled carrier diffusion by maintaining the interparticle distance with the homogenous four-fold symmetry.

3. Summary

We demonstrate stable halide perovskite SC preparation by bidentate ligand exchange on PNCs. STEM images, XRD patterns, and SAXS data suggest that the bidentate ligand maintains the nanocrystal ordered in an SC. Fast Fourier transform (FFT) analyses of STEM or SEM images and SAXS data show long-range nanocrystal periodicity in an SC than in a film with randomly arranged PNCs. The emission wavelength and lifetime of SCs are closer to isolated PNCs than a

PNC film with largely red-shifted emission and delayed carrier recombination. Unlike an increase in the non-geminate recombination rate in a PNC film, the bidentate ligand maintains the PNC identity in an SC, rendering stronger quantum confinement. These results suggest stable perovskite SCs prepared using bidentate ligands overcome undesired exciton splitting and carrier recombination.

4. Experimental Section

Materials: We used the following chemicals without further purification. Cesium acetate (Sigma-Aldrich, 99.9%), Cesium carbonate (Sigma-Aldrich, 99.9%), oleylamine (TCI, >50.0%), $PbBr_2$ (Sigma-Aldrich, ≥98.0%), oleic acid (TCI, >85.0%), hexadecyl amine (Fujifilm Wako), eicosanedioic acid (TCI, >98.0%), 1-hexadecene (Fujifilm Wako), 1-octadecene (Fujifilm Wako), and dehydrated toluene (Fujifilm Wako, >99.5%).

Synthesis of $CsPbBr_3$ perovskite nanocrystals (PNCs): A mixture of $PbBr_2$ (420 mg, 1.1 mmol), oleic acid (3.2 mL, 10 mmol), hexadecyl amine (2.4 g, 10 mmol), and 1-hexadecene (50 mL) was added into a three-necked flask and heated at 120 ℃ under a vacuum for 1 h. Parallely, a mixture of cesium acetate (30 mg, 0.15 mmol), 1-hexadecene (1.2 mL), and oleic acid (180 μL, 0.5 mmol) in another three-necked flask was heated at 120 ℃ under a vacuum for 1 h. After all the precursors were dissolved, the temperature was increased to 170 ℃, and Ar gas was flushed for 30 min. The hot cesium acetate solution was injected into the $PbBr_2$ solution within a few seconds. Immediately (within 1 min), the reaction mixture was cooled in an ice-water bath. 50 mL of toluene was added into the as-synthesized $CsPbBr_3$ PNC colloid, and the solution was centrifuged at 14500 rpm for 30 min. The supernatant was discarded, and the precipitate was redispersed in toluene. The PNC

colloid was centrifuged at 2000 rpm for 5 min to separate large PNCs and aggregates. The supernatant was collected and used in this study.

Synthesis of $CsPbI_3$ PNCs: A mixture of PbI_2 (1.734 g, 3.8 mmol), oleic acid (1 mL, 3.2 mmol), oleylamine (1 mL, 3.0 mmol), and 1-octadecane (10 mL) was added into a two-necked flask and heated at 120 ℃ under a vacuum for 1 h. Parallely, a mixture of cesium carbonate (162.8 mg, 0.5 mmol), oleic acid (0.5 mL, 1.6 mmol), and 1-octadecane (8 mL) was loaded in another two-necked flask and heated at 120 ℃ under a vacuum for 1 h. After all the precursors were dissolved, the temperature was increased to 160 ℃, and Ar gas was flushed for 30 min. The hot cesium oleate solution (0.8 mL) was injected into the PbI_2 solution within a few seconds. Immediately (within 1 min), the reaction mixture was cooled in the ice-water bath. The solution was centrifuged at 6000 rpm for 10 min. The residue was redispersed in toluene and centrifuged again at 12000 rpm for 10 min. The supernatant was discarded, and the precipitate was redispersed in toluene. The PNC colloid was centrifuged at 2000 rpm for 5 min to separate large PNCs and aggregates. The supernatant was collected and used in this study.

Synthesis of $CsPbBr_3$ SCs: First, a solution (0.5 mM) of eicosanedioic acid [EA, $(CH_2)_{18}(COOH)_2$] was prepared in toluene. This solution was added to 2 mL of the $CsPbBr_3$ PNC colloid in toluene. The mixture was undisturbed for 2 days at 25 ℃ in a screw-cap bottle. The supernatant of the sample was decanted and discarded. The settled SCs were washed with the 0.5 mM EA solution in toluene.

PL decay recording: Time-resolved PL measurements were carried out on an inverted optical microscope (IX71, OLYMPUS). The excitation light was femtosecond laser pulses (405 nm, 150 fs, 200 kHz) generated from the SHG crystal of an optical parametric amplifier (Coherent OPA-

9400). The PL from the sample was collected using a 40x objective lens and filtered through a 420 nm long-pass filter. Time-resolved PL spectra were recorded for 2 min using an assembly of a polychromator (model 250IS, Chromex) and a Streak-camera (model C4334, Hamamatsu). The average power of the fs laser pulses (~8 mW) was controlled with 0.1-10% ND filters before passing through the focusing lens placed before the sample. Also, we used a single photon counting system for PL decay measurements, which was equipped with an avalanche photodiode (Perkin Elmer, SPCM-AQRH)-time-correlated single photon counting module system (Becker & Hickl GmbH, SPC-830). The excitation light source in the ps system was a Hamamatsu PLP-10 pulsed laser (405 nm, 60 ps, 1 MHz). Amplitude-weighted average PL lifetimes $\tau_{amp.}$ were calculated by the equation: $\tau_{amp.} = (A_1\tau_1^2+A_2\tau_2^2+A_3\tau_3^2)/ (A_1\tau_1+A_2\tau_2+A_3\tau_3)$.

Characterization of PNCs and SCs: The absorption and steady-state PL spectra of purified $CsPbX_3$ PNC colloid were recorded using a UV-vis spectrophotometer (Evolution 220, Thermo Fischer Scientific) and a fluorescence spectrometer (F-4500, Hitachi). The morphologies of the the PNCs, PNC films, and SCs were examined using a STEM (HD-2000 microscope, HITACHI) operated at 200 kV. STEM samples were prepared by drop-casting the PNC colloid or SC suspensions on copper grids supported by carbon films (Okenshoji). The top view and cross-section images of PNC films were recorded using an SEM (SU8230, HITACHI) operated at 1 kV. The size distributions of PNCs and FFT images were obtained by the NIH ImageJ 1.48 v package. XRD and SAXS profiles of PNCs and SCs were recorded on an X-ray diffractometer (SmartLab, RIGAKU) with a Cu Kα (λ = 0.15406 nm) X-ray source. Samples were deposited on glass slides and Kapton films for XRD and SAXS measurements.

Investigation of mechanical stability of PNC films and SCs: To examine the mechanical stability of the EA-assisted PNC SCs, we measured STEM and SEM images, PL spectra, PL

decays of PNC films, and SCs before and after applying a lateral mechanical force of ≥ 5 N. The mechanical force was applied as follows. Firstly, a PNC film or dispersed SCs deposited on a glass coverslip were covered by a glass slide. The lateral force was applied by fixing the lower glass coverslip to a table, pushing the glass slide vertically, and sliding the upper glass slide. Figures S7 and S8 show the morphologies of a close-packed PNC film and an SC before and after the mechanical deformation. The film showed a large PL blueshift (Figure 4c) and a decrease in the PL lifetime (from 106 ns to 84.3 ns, Figure S7c,d) by applying mechanical force. Conversely, the mechanical force did not greatly affect the PL spectral maximum (Figure 4d) or the lifetime (Figure S8c,d) of an SC. Interestingly, the SC showed a PL redshift ($\Delta\lambda$ = 3 nm) with an increase in the PL lifetime (from 7.4 ns to 13.8 ns). The PL blueshift and PL lifetime decrease for the PNC film suggest assembly dissociation. The PL spectral redshift and lifetime increase for the SC suggest the partial (surface, Figure S8) structural change of SCs to an NC film.

Acknowledgements

This research was supported by the MEXT JSPS Grants 20J00974, 21K14580 and 19H02550. We acknowledge the Hokkaido University Nanotechnology PLATFORM.

Conflict of Interest

The authors declare no conflict of interest.

Data Availability Statement. The data (Figures S1-S8, and Table S1) supporting this study are available in the supplementary material of this article.

Keywords: halide perovskites • supercrystal • nanocrystals • self-assembly • exciton

[1] a) Kojima, K. Teshima, Y. Shirai, T. Miyasaka, *J. Am. Chem. Soc.* **2009**, *131*, 6050–6051; b) L. Chouhan, S. Ghimire, C. Subrahmanyam, T. Miyasaka, V. Biju, *Chem. Soc. Rev.* **2020**, *49*, 2869–2885; c) A. Dey, J. Ye, A. De, E. Debroye, S. K. Ha, E. Bladt, A. S. Kshirsagar, Z. Wang, J. Yin, Y. Wang, *et al., ACS Nano* **2021**, *15*, 10775–10981; d) R. Su, Z. Xu, J. Wu, D. Luo, Q. Hu, W. Yang, X. Yang, R. Zhang, H. Yu, T. P. Russell, *et al., Nat. Commun.* **2021**, *12*; e) S. Nanz, R. Schmager, M. G. Abebe, C. Willig, A. Wickberg, A. Abass, G. Gomard, M. Wegener, U. W. Paetzold, C. Rockstuhl, *APL Photon.* **2019**, *4*, 076104; f) J. Song, J. Li, X. Li, L. Xu, Y. Dong, H. Zeng, *Adv. Mater.* **2015**, *27*, 7162–7167; g) Y. Cai, W. Li, D. Tian, S. Shi, X. Chen, P. Gao, R.-J. Xie, *Angew. Chem.Int. Ed.* **2022**, *61*, e202209880.

[2] J. M. Pietryga, Y.-S. Park, J. Lim, A. F. Fidler, W. K. Bae, S. Brovelli, V. I. Klimov, *Chem. Rev.* **2016**, *116*, 10513–10622.

[3] J. K. Pious, C. Muthu, S. Dani, A. Saeki, C. Vijayakumar, *Chem. Mater.* **2020**, *32*, 2647–2652.

[4] P. Zeng, X. Ren, L. Wei, H. Zhao, X. Liu, X. Zhang, Y. Xu, L. Yan, K. Boldt, T. A. Smith, et al. *Angew. Chem.* **2022**, *134*, e202111443.

[5] J. Wu, J. Tong, Y. Gao, A. Wang, T. Zhang, H. Tan, S. Nie, Z. Deng, *Angew. Chemi. Int. Ed.* **2020**, *59*, 7738–7742.

[6] Q. Q. Fan, G. V. Biesold-McGee, J. Z. Ma, Q. N. Xu, S. Pan, J. Peng, Z. Q. Lin, *Angew. Chem. Int. Ed.* **2020**, *59*, 1030–1046.

[7] S. Ghimire, L. Chouhan, Y. Takano, K. Takahashi, T. Nakamura, K.-I. Yuyama, V. Biju,

ACS Energy Lett. **2019**, *4*, 133–141.

[8] J. Liu, X. Zheng, O. F. Mohammed, O. M. Bakr, *Acc. Chem. Res.* **2022**, *55*, 262–274.

[9] a) G. Rainò, M. A. Becker, M. I. Bodnarchuk, R. F. Mahrt, M. V. Kovalenko, T. Stöferle, *Nature* **2018**, *563*, 671–675; b) C. Zhou, Y. Zhong, H. Dong, W. Zheng, J. Tan, Q. Jie, A. Pan, L. Zhang, W. Xie, *Nat. Commun.* **2020**, *11*, 329.; c) F. Krieg, P. C. Sercel, M. Burian, H. Andrusiv, M. I. Bodnarchuk, T. Stöferle, R. F. Mahrt, D. Naumenko, H. Amenitsch, G. Rainò, et al., *ACS Cent. Sci.* **2021**, *7*, 135–144; d) I. Cherniukh, T. V. Sekh, G. Rainò, O. J. Ashton, M. Burian, A. Travesset, M. Athanasiou, A. Manoli, R. A. John, M. Svyrydenko, et al., *ACS Nano* **2022**, *16*, 7210–7232.

[10] a) C. Zhou, J. M. Pina, T. Zhu, D. H. Parmar, H. Chang, J. Yu, F. Yuan, G. Bappi, Y. Hou, X. Zheng, et al., *Adv. Sci.* **2021**, *8*, 2101125; b) D. Vila-Liarte, M. W. Feil, A. Manzi, J. L. Garcia-Pomar, H. Huang, M. Döblinger, L. M. Liz-Marzán, J. Feldmann, L. Polavarapu, A. Mihi, *Angew. Chem. Int. Ed.* **2020**, *59*, 17750–17756.

[11] a) J. Jagielski, S. Kumar, M. Wang, D. Scullion, R. Lawrence, Y. T. Li, S. Yakunin, T. Tian, M. V. Kovalenko, Y. C. Chiu, et al., *Sci. Adv.* **2017**, *3*, eaaq0208; b) C. Bi, S. Wang, S. V. Kershaw, K. Zheng, T. Pullerits, S. Gaponenko, J. Tian, A. L. Rogach, *Adv. Sci.* **2019**, *6*, 1900462; c) Z. Zhang, S. Ghimire, T. Okamoto, B. M. Sachith, J. Sobhanan, C. Subrahmanyam. V. Biju, *ACS Nano.* **2022**, *16*, 160–168.

[12] a) D. Baranov, S. Toso, M. Imran, L. Manna, *J. Phys. Chem. Lett.* **2019**, *10*, 655–660; b) Y. Tang, D. Poonia, M. Van Der Laan, D. Timmerman, S. Kinge, L. D. A. Siebbeles, P. Schall, *ACS Appl. Energy Mater.* **2022**, *5*, 5415–5422.

[13] M. C. Weidman, A. J. Goodman, W. A. Tisdale, *Chem. Mater.* **2017**, *29*, 5019–5030.

[14] a) Y. Tong, E.-P. Yao, A. Manzi, E. Bladt, K. Wang, M. Döblinger, S. Bals, P. Müller-

Buschbaum, A. S. Urban, L. Polavarapu, *et al*., *Adv. Mater.* **2018**, *30*, 1801117; b) H. D. Guo, Y. Y. Fang, H. B. Cheng, J. P. Wu, Y. Lei, S. M. Wang, X. R. Li, Y. H. Dai, W. C. Xiang, D. J. Xue, *Angew. Chem.Int. Ed.* **2022**, *61*, e202204148.; c) D. Baranov, A. Fieramosca, R. X. Yang, L. Polimeno, G. Lerario, S. Toso, C. Giansante, M. D. Giorgi, L. Z. Tan, D. Sanvitto, *et al., ACS Nano*, **2021**, *15,* 650–664; d) Q. R. Cheng, H. Y. Chen, F. Yang, Z. Y. Chen, W. J. Chen, H. Y. Yang, Y. X. Shen, X. M. Ou, Y. Y. Wu, Y. W. Li, *Angew. Chem.Int. Ed.* **2022**, *61*, e202210613.

[15] C. R. Kagan, C. B. Murray, *Nat. Nanotech.* **2015**, *10*, 1013–1026.

[16] D. Luo, X. Qin, Q. Song, X. Qiao, Z. Zhang, Z. Xue, C. Liu, G. Mo, T. Wang, *Adv. Funct. Mater.* **2017**, *27*, 1701982.

[17] Y. Liu, M. Siron, D. Lu, J. Yang, R. Dos Reis, F. Cui, M. Gao, M. Lai, J. Lin, Q. Kong, *et al*., *J. Am. Chem. Soc.* **2019**, *141*, 13028–13032.

[18] J. S. Van Der Burgt, J. J. Geuchies, B. Van Der Meer, H. Vanrompay, D. Zanaga, Y. Zhang, W. Albrecht, A. V. Petukhov, L. Filion, S. Bals, *et al*., *J. Phys. Chem. C* **2018**, *122*, 15706–15712.

[19] K.-H. Wang, J.-N. Yang, Q.-K. Ni, H.-B. Yao, S.-H. Yu, *Langmuir* **2018**, *34*, 595–602.

[20] Y. Tang, L. Gomez, A. Lesage, E. Marino, T. E. Kodger, J.-M. Meijer, P. Kolpakov, J. Meng, K. Zheng, T. Gregorkiewicz, *et al*., *Nano Lett.* **2020**, *20*, 5997–6004.

[21] E. Cao, J. Qiu, D. Zhou, Y. Yang, Q. Wang, Y. Wen, *Chem. Commun.* **2020**, *56*, 4460–4463.

[22] S. Wang, L. Zhou, F. Huang, Y. Xin, P. Jin, Q. Ma, Q. Pang, Y. Chen, J. Z. Zhang, *J. Mater. Chem. C* **2018**, *6*, 10994–11001.

[23] H. Li, X. Liu, Q. Ying, C. Wang, W. Jia, X. Xing, L. Yin, Z. Lu, K. Zhang, Y. Pan, *et al*.,

Angew. Chem. **2020**, *132*, 17360–17366.

[24] L. Protesescu, S. Yakunin, M. I. Bodnarchuk, F. Krieg, R. Caputo, C. H. Hendon, R. X. Yang, A. Walsh, M. V. Kovalenko, *Nano Lett.* **2015**, *15*, 3692–3696.

[25] L. M. Pazos-Outón, M. Szumilo, R. Lamboll, J. M. Richter, M. Crespo-Quesada, M. Abdi-Jalebi, H. J. Beeson, M. Vrućinić, M. Alsari, H. J. Snaith, *et al*., *Science*, **2016**, *351*, 1430–1433.

[26] J. A. Sichert, A. Hemmerling, C. Cardenas-Daw, A. S. Urban, J. Feldmann, *APL Mater.* 2019, 7, 041116.

[27] G. E. Eperon, E. Jedlicka, D. S. Ginger, *J. Phys. Chem. Lett.* **2018**, *9*, 104–109.

[28] J. Maes, L. Balcaen, E. Drijvers, Q. Zhao, J. De Roo, A. Vantomme, F. Vanhaecke, P. Geiregat, Z. Hens, *J. Phys. Chem. Lett.* **2018**, *9*, 3093–3097.

[29] H.-H. Fang, L. Protesescu, D. M. Balazs, S. Adjokatse, M. V. Kovalenko, M. A. Loi, *Small* **2017**, *13*, 1700673.

[30] K. Cho, H. Tahara, T. Yamada, H. Suzuura, T. Tadano, R. Sato, M. Saruyama, H. Hirori, T. Teranishi, Y. Kanemitsu*, Nano Lett.* **2022**, *22*, 7674–7681.

[31] D. Lapkin, C. Kirsch, J. Hiller, D. Andrienko, D. Assalauova, K. Braun, J. Carnis, Y. Y. Kim, M. Mandal, A. Maier, *et al*., *Nat. Commun.* **2022**, *13*, 892.

Figures

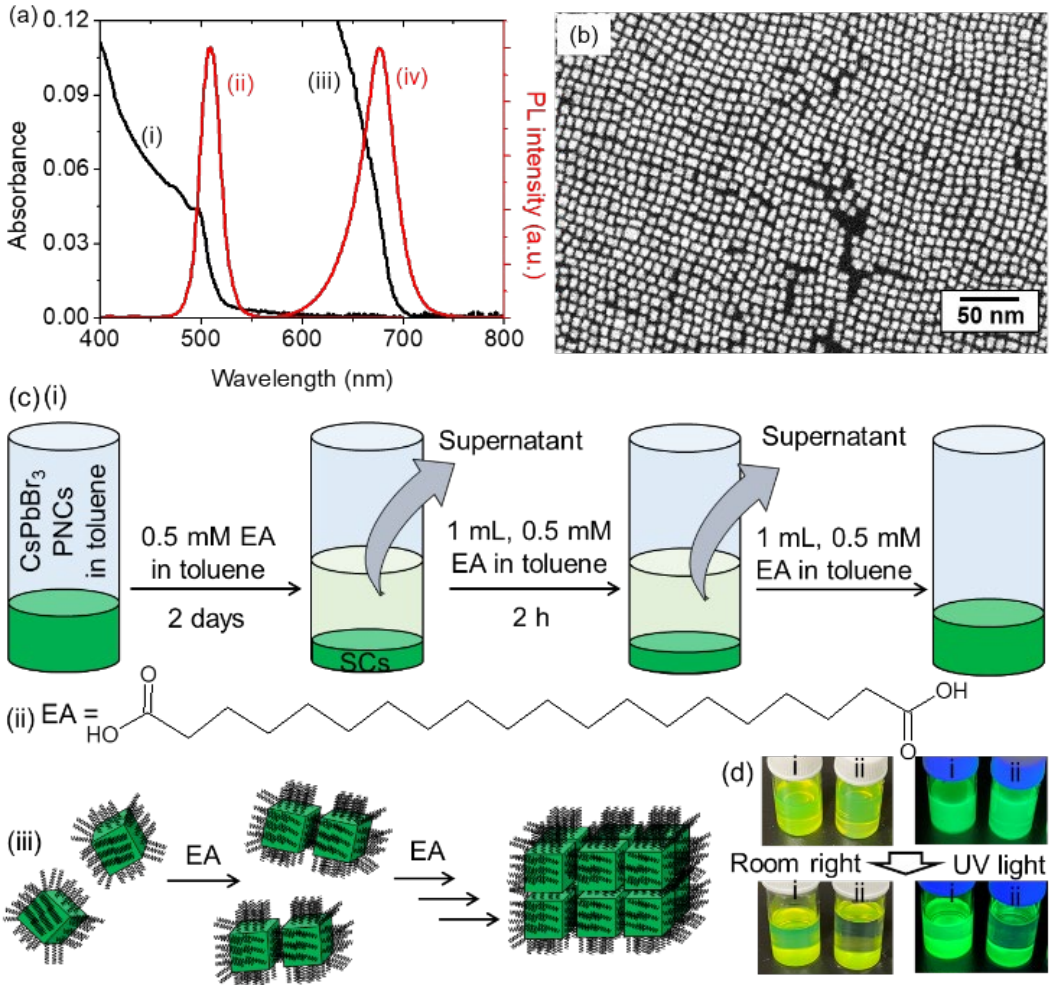

Figure 1. (a) The absorption (i,iii) and PL (ii,iv) spectra of as-synthesized $CsPbBr_3$ and $CsPbI_3$ PNC samples dispersed in toluene. (b) STEM image of $CsPbBr_3$ PNCs (also, see Figure S2). (c) A scheme of (i) $CsPbBr_3$ SC preparation, (ii) EA, and (iii) SC formation. (f) The photographs of $CsPbBr_3$ NC colloidal solutions (i) without and (ii) with adding an EA solution.

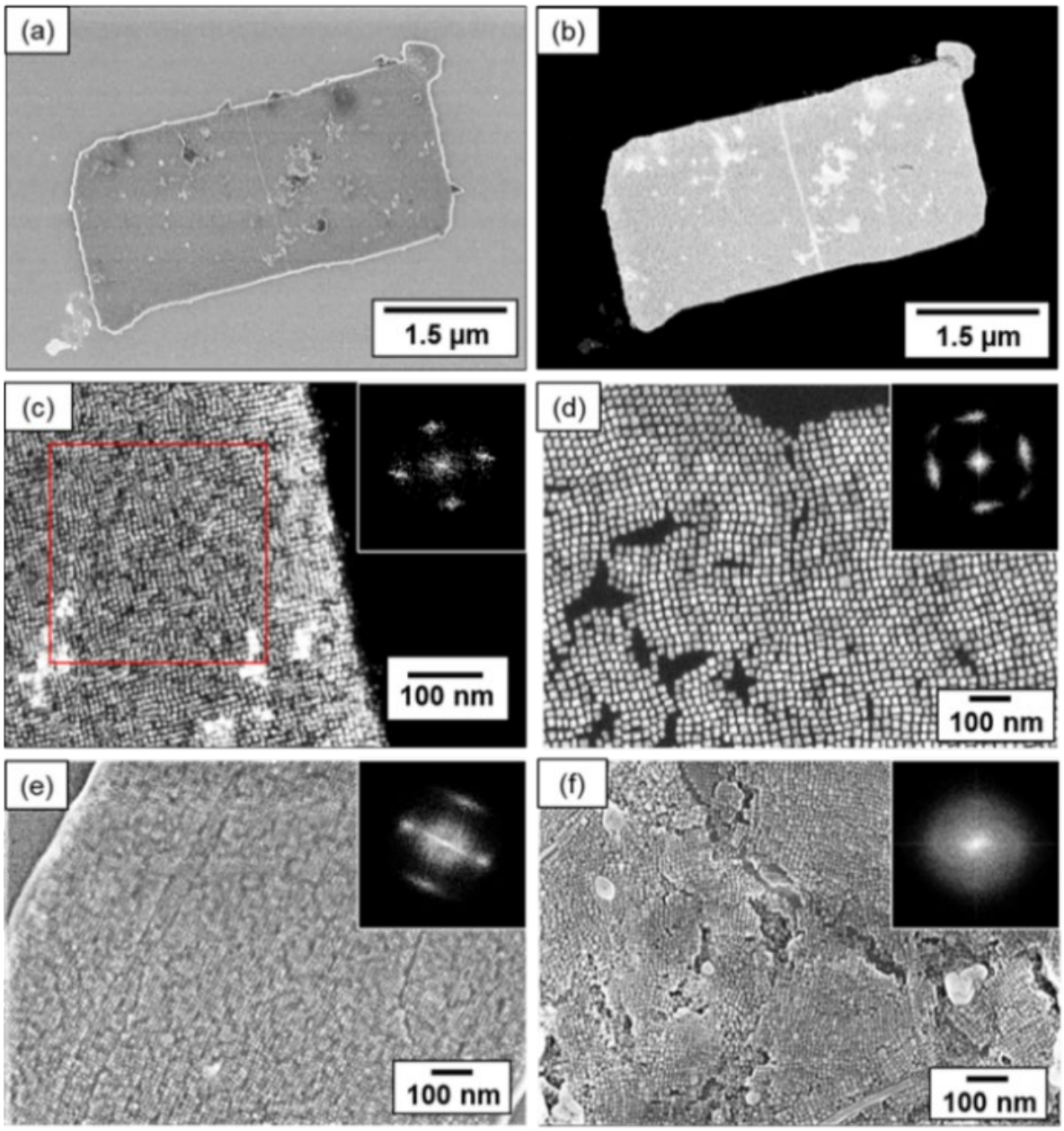

Figure 2. (a,e,f) SEM and (b,c,d) STEM images of $CsPbBr_3$ (a-c,e) SCs, (d) 2D self-assembled monolayer of PNCs, and (f) a PNC film. The images d-f were recorded at 100k magnification. Insets in c-f are the corresponding FFT data.

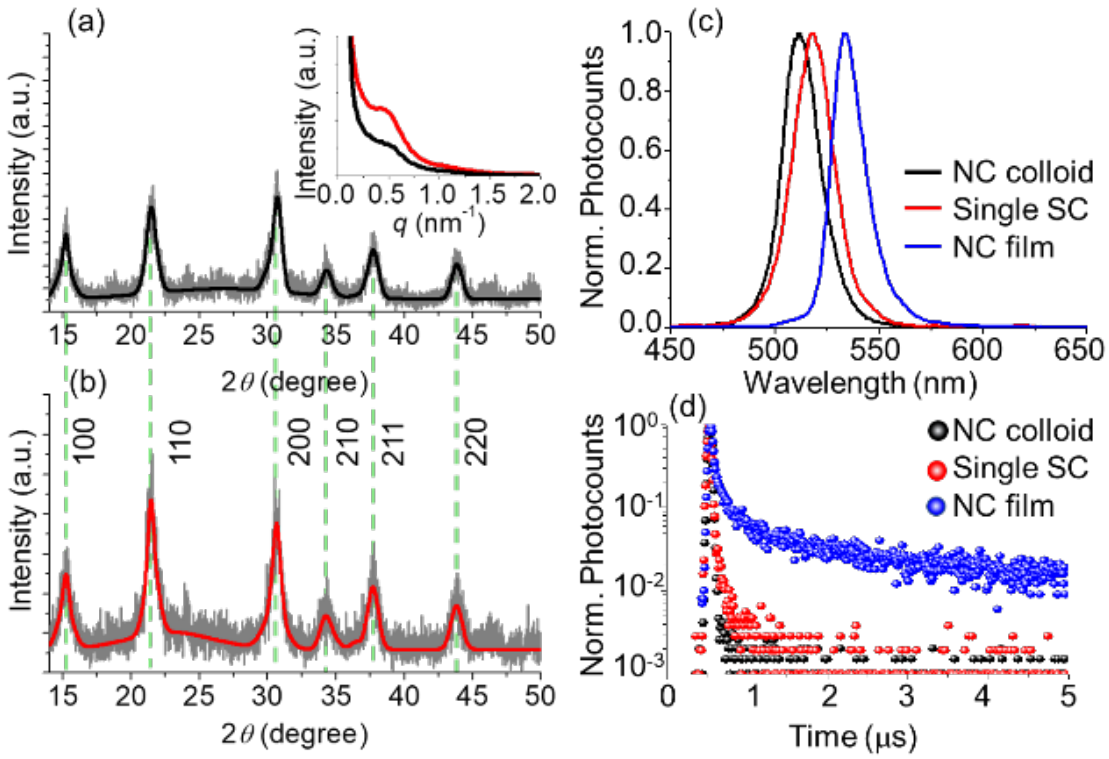

Figure 3. (a,b) XRD patterns of (a) a $CsPbBr_3$ PNC film and (b) SCs. Inset: SAXS data for (black line) a PNC film and (red line) SCs. (c) PL spectra and (d) PL decays of a $CsPbBr_3$ PNC colloidal solution, single SC, and a PNC film. The excitation laser fluence is 3 nJ cm^{-2} and λ_{ex} = 405 nm.

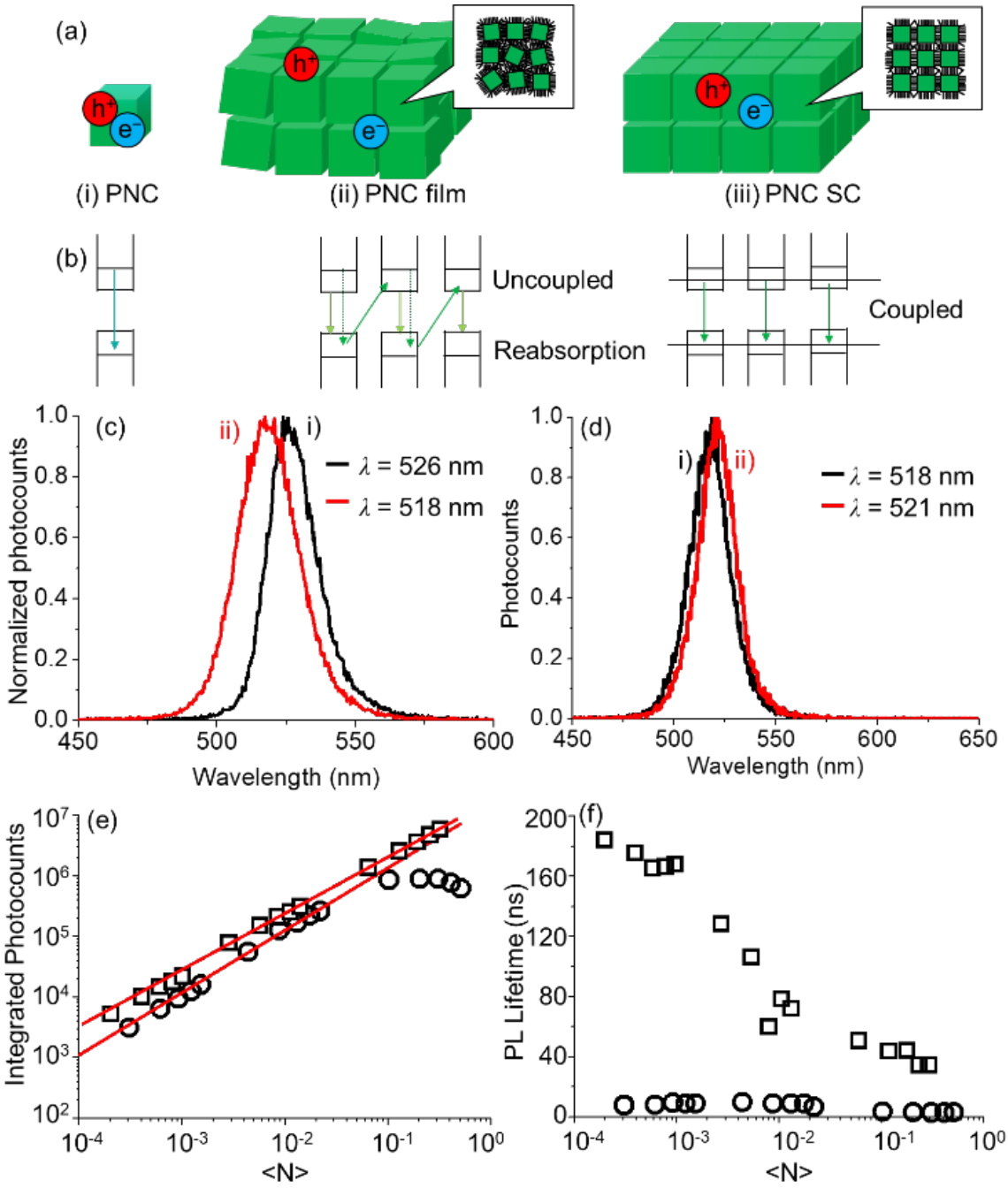

Figure 4. (a,b) Schemes of exciton confinement, miniband formation, and reabsorption in (i) a PNC, (ii) a PNC film and (iii) an SC. (c,d) Plots of (c) photocounts and (d) PL lifetimes vs. $\langle N \rangle$ of (□) an $CsPbBr_3$ PNC film and (○) an SC. The plots of integrated photocounts are fitted to $I_{ex}^{k} = B \langle N \rangle^{k}$ (red lines).

Table of Contents Entry

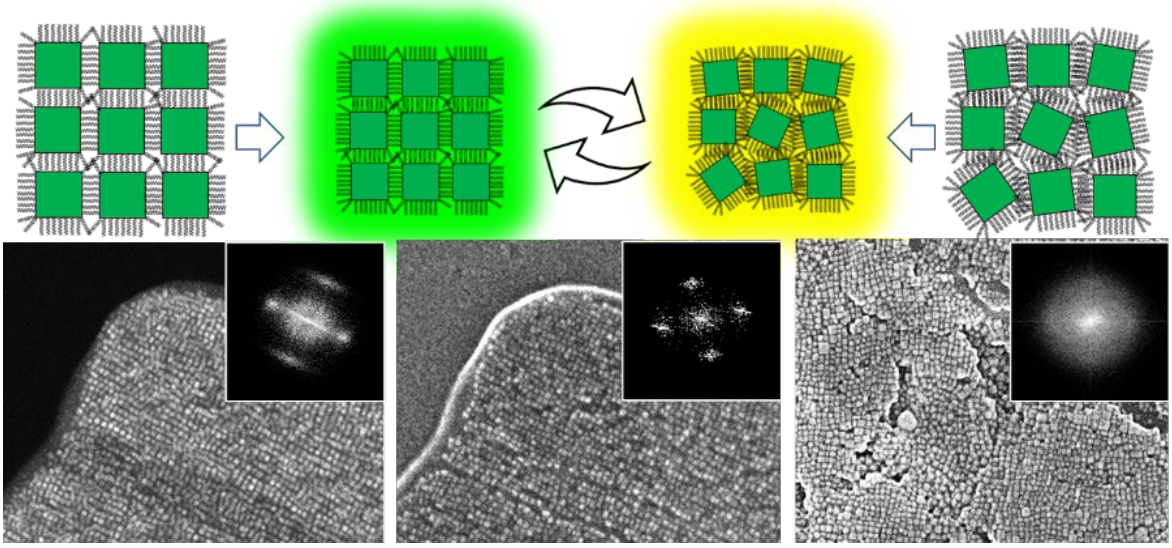

ToC text:

Using bidentate ligands, halide perovskite supercrystals are prepared by ligand-exchange-assisted long-range and high-order nanocrystal assembling. The resulting 2D and 3D supercrystals retain quantum confinement and excitonic properties different from exciton splitting, carrier trapping, and charge diffusion in a perovskite film with randomly arranged nanocrystals. This method offers a route to supercrystal fabrication for light-emitting and light-harvesting devices